Expert Systems with Applications 37 (2010) 288–297

Contents lists available at ScienceDirect

Expert Systems with Applications

journal homepage: www.elsevier.com/locate/eswa

# Locally edge-adapted distance for image interpolation based on genetic fuzzy system

Hsiang-Chieh Chen [a], Wen-June Wang [a,b,*]

[a] Department of Electrical Engineering, National Central University, Jhongli City, Taoyuan County 32001, Taiwan, ROC
[b] Department of Electrical Engineering, National Taipei University of Technology, Taipei 10608, Taiwan, ROC

ARTICLE INFO

*Keywords:*
Fuzzy logic
Genetic algorithm
Image interpolation
Image zooming

ABSTRACT

This study presents a new adaptive scheme for developing kernel-based interpolation methods that simultaneously enhance spatial image resolution and preserve locally detailed edges. A new edge-adapted distance is first estimated according to local gradients information by combining fuzzy theory with genetic learning algorithm. This estimated distance is then employed in place of the original Euclidean distance in various interpolation methods. Additionally, a learning procedure based on genetic algorithm is presented to obtain crucial parameters of the fuzzy system automatically. Experimental results presented in numerical comparisons and in visual observations verify the effectiveness of the proposed adaptive framework for kernel-based interpolation methods.



## 1. Introduction

Interpolation is an extensively adopted research method for estimating intermediate data points within a set of discrete samples (Lehmann, Gönner, & Spitzer, 1999; Meijering & Unser, 2003; Reichenbach & Geng, 2003; Tafti, Shirani, & Wu, 2006). In signal/image processing subfields, interpolation is the process of defining a spatially continuous signal or image from several sampled data, and re-sampling at a specified point. The interpolation methods are generally implemented by convolving available samples with a finite-size kernel. Hence, the interpolated value at a specified point can be considered as a weighted sum of the neighboring samples. Most interpolation methods have a trade-off between computational complexity and reproduction quality (El-Khamy, Hadhoud, Dessouky, Salam, & Abd El-Samie, 2005). The basic methods most commonly used in image, video and multimedia products are nearest neighbor, bilinear, cubic convolution (Keys, 1981; Shi & Reichenbach, 2006), and cubic spline interpolation methods (Lehmann et al., 1999).

The sinc function is a theoretically ideal interpolator to reconstruct the continuous function according to information theory. However, this interpolator has an infinite impulse response, and is not appropriate for local interpolation in practical applications. Several polynomial forms, such as the well-known Lagrange and Gaussian polynomials, have been presented to approximate the sinc function. The kernel type formed with polynomials accomplishes more accurate results than linear-based methods, but needs a long execution time because the size of convolution kernel is large. The family of cubic convolution kernels provides a primary solution to the trade-off between computational complexity and interpolation accuracy (Keys, 1981; Reichenbach & Geng, 2003). Moreover, wavelet-based methods are also often adopted in image interpolation. A wavelet-domain method to estimate detail wavelet coefficients at high resolution scales has been presented (Temizel & Vlachos, 2006). The method wavelet exploits coefficient correlation in local neighborhood, and adopts linear least-squares regression to obtain wavelet coefficients. Chang, Cvetković, and Vetterli (2006) presented an algorithm that adopts a wavelet transform to extract the information of sharpness variations in low-resolution (LR) images. The information is then adopted to estimate high-frequency properties to preserve the sharpness of edges in enlarged high-resolution (HR) images. The limitation of wavelet-based methods is that they cannot select the non-integer magnification factor.

Some nonlinear interpolation methods have recently been presented to reconstruct HR images with intelligent schemes. These approaches include neural networks (Plaziac, 1999; Sigitani, Iiguni, & Maeda, 1999), optimal recovery (Muresan & Parks, 2004) and vector quantization theory (Hong, Park, Yang, & Kim, 2008; Sheppard, Panchapakesan, Bilgin, Hunt, & Marcellin, 2000). The quality of a reconstructed image depends strongly on the estimation accuracy, particularly when the interested point is around the sharp region. Edge-based methodologies have been introduced in many investigations (Aràndiga, Donat, & Mulet, 2003; Battiato, Gallo, & Stanco, 2002; Carey, Chuang, & Hemami, 1999; Carrato, Ramponi, & Marsi, 1996; Carrato & Tenze, 2000; Cha & Kim, 2007; Chen, Huang, & Lee, 2005; Huang & Lee, 2004; Li & Orchard, 2001; Wang

* Corresponding author. Address: Department of Electrical Engineering, National Central University, No. 300, Jhongda Road, Jhongli City, Taoyuan County 32001, Taiwan, ROC. Tel.: +886 3 4227151x34456; fax: +886 3 4255830.
*E-mail address:* wjwang@ee.ncu.edu.tw (W.-J. Wang).

0957-4174/$ - see front matter © 2009 Elsevier Ltd. All rights reserved.
doi:10.1016/j.eswa.2009.05.069

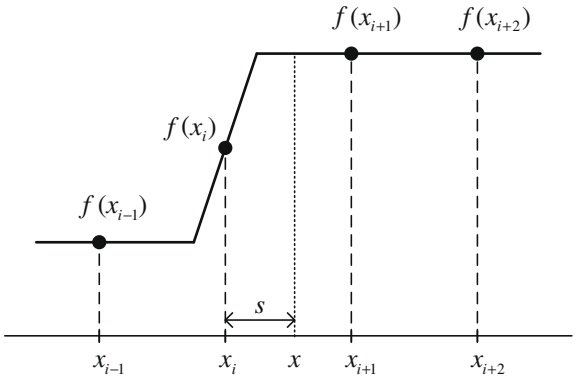


**Fig. 1.** Ideal edge model in 1D case.

& Ward, 2007; Zhang & Wu, 2006). Accordingly, the primary novelty underlying this study is to enhance the effectiveness of a specified image interpolation method, especially for locally detailed edges, by employing intelligent scheme.

To enhance the spatial quality of enlarged HR images, this study presents an adaptive framework to improve the effectiveness of traditional interpolation methods. By combining fuzzy theory with genetic learning algorithm, an adaptive distance based on local gradients information is obtained to replace the original Euclidean distance of interpolation formulae. The adaptive distance reduces the interpolation error at the position around the edges, and is applicable to various interpolation methods that utilize kernels to calculate the weights of involved samples. This study also discusses ways of determining the fuzzy system parameters, and of accelerating the procedure of the proposed algorithm. Simulation results demonstrate that the proposed adaptive scheme enhances the performance of the specified interpolation methods on spatial resolution enhancement of images.

The rest of this paper is organized as follows. Section 2 introduces a review of interpolation and describes the motivation underlying this work. Section 3 then presents the principal configuration of the proposed algorithm. Next, Section 4 provides detailed discussions and comparisons of simulation results involving commonly used images. Conclusions are finally drawn in Section 5.

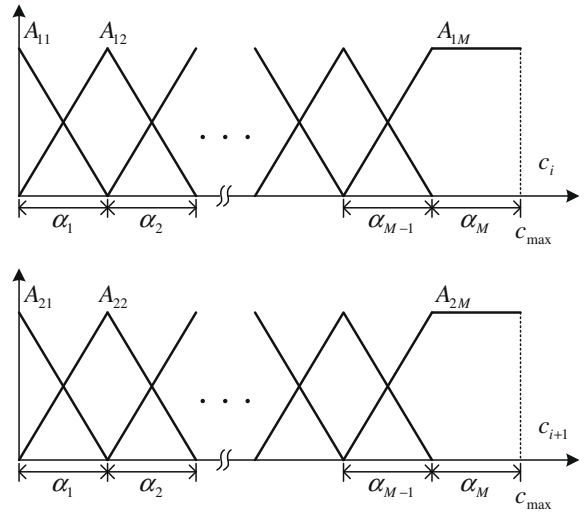


**Fig. 3.** Fuzzy sets of the premise variables.

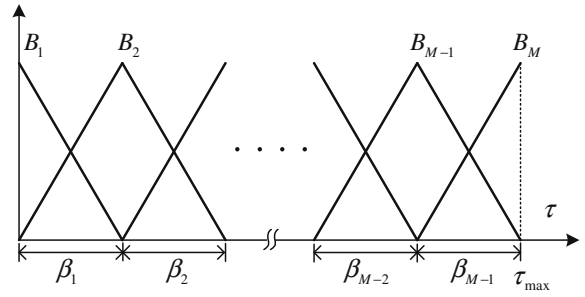


**Fig. 4.** Fuzzy sets of the consequent variable.

**Table 1**
Predefined fuzzy rule table.

| $c_{i+1}$ \ $c_i$ | $A_{11}$ | $A_{12}$ | ... | $A_{1M}$ |
|---|---|---|---|---|
| $A_{21}$ | $B_1$ | $B_2$ | ... | $B_M$ |
| $A_{22}$ | $B_2$ | $B_1$ | ... | $B_{M-1}$ |
| ⋮ | ⋮ | ⋮ | ⋱ | ⋮ |
| $A_{2M}$ | $B_M$ | $B_{M-1}$ | ... | $B_1$ |

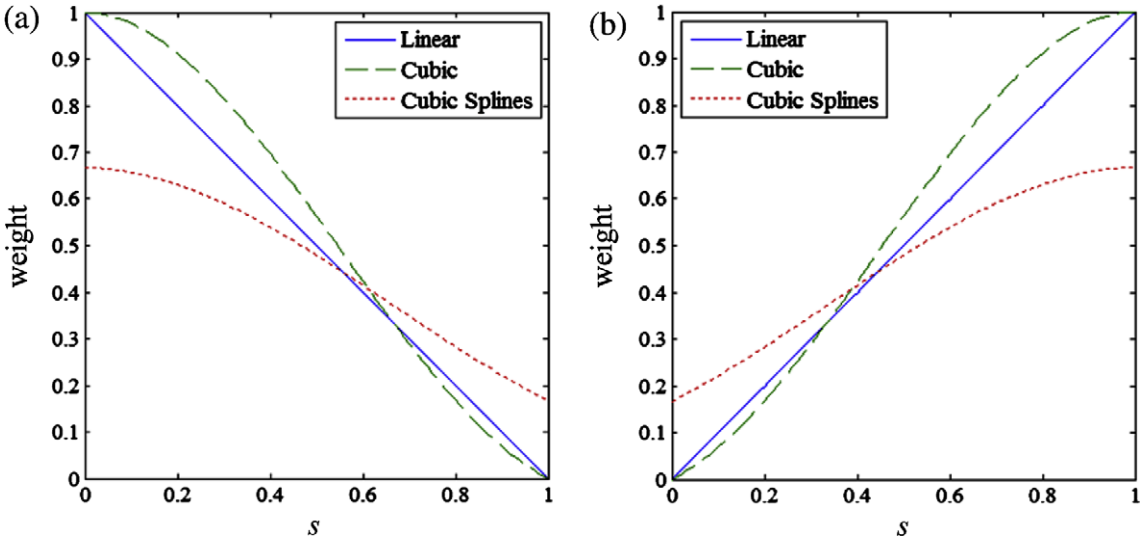


**Fig. 2.** Relationship between $s$ and the weight of: (a) $f(x_i)$ and (b) $f(x_{i+1})$.

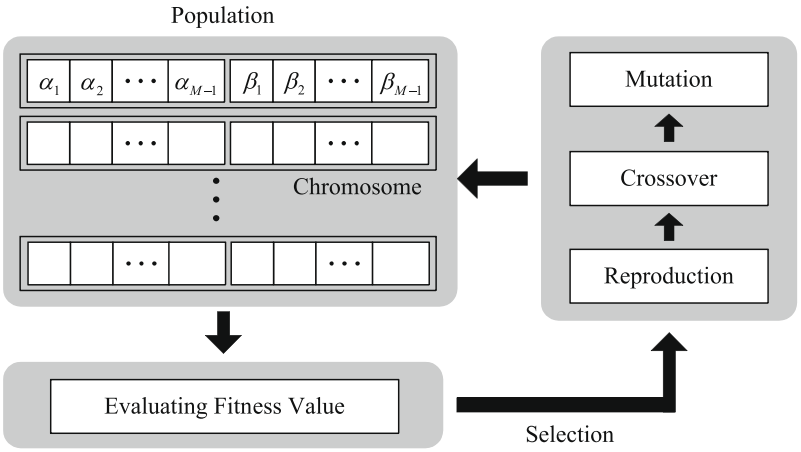


**Fig. 5.** Diagram of the genetic algorithm.

**Table 2**
Deterministic parameters optimized by genetic learning algorithm.

| Methods | No. of labels | Base length of premise variable | Base length of consequent variable |
|---|---|---|---|
| Bilinear | $M = 3$ | $\alpha_1 = 40$, $\alpha_2 = 32$ | $\beta_1 = 0.16$, $\beta_2 = 0.13$ |
| Bicubic | $M = 5$ | $\alpha_1 = 26$, $\alpha_2 = 27$, $\alpha_3 = 19$, $\alpha_4 = 17$ | $\beta_1 = 0.07$, $\beta_2 = 0.05$, $\beta_3 = 0.03$, $\beta_4 = 0.04$ |
| Cubic Spline | $M = 3$ | $\alpha_1 = 43$, $\alpha_2 = 37$ | $\beta_1 = 0.18$, $\beta_2 = 0.13$ |

## 2. Preliminaries

### 2.1. Traditional interpolation methods

Image interpolation that attempts to build a continuous two-dimensional image from discrete samples is a key step to achieving high-qualified image resolution. In practice, symmetrical and separable interpolation kernels are often adopted to reduce the implementation burden. Hence, interpolation in images can be performed sequentially row-wise and column-wise. For simplicity and without loss of generality, the remainder of this study develops the proposed algorithm with respect to one-dimensional (1D) case. A point $x$ is interpolated by convolving discrete samples $f(x_k)$ with a kernel $\varphi$ to define the continuous result $\tilde{f}$

$$\tilde{f}(x) = \sum_k f(x_k)\varphi\left(\frac{x - x_k}{h}\right), \tag{1}$$

where $h$ denotes the sampling increment, and $x_k$ denotes a sampling node. Suppose that point $x$ exists in the interval $[x_i, x_{i+1}]$, and the normalized Euclidean distance (NED) is $s = (x - x_i)/h$ $(0 \leqslant s \leqslant 1)$. Since $(x - x_k)/h = (x - x_i + x_i - x_k)/h = s + (x_i - x_k)/h$ and $(x_i - x_k) = (i - k)h$, Eq. (1) is reformulated as

$$\tilde{f}(x) = \sum_k f(x_k)\varphi(s + i - k). \tag{2}$$

Hence, the interpolation kernel $\varphi$ converts discrete data into a continuous function by a convolution-like operation defined in Eq. (2). An ideal model of interpolation kernel is the sinc function. However, the interpolation kernel is not practical to images due to its spatially infinite size. Accordingly, numerous kernels have been presented to maximize interpolation effectiveness for a given level of computation complexity. The simplest method is to approximate sinc function by a triangular function

$$\varphi_1(u) = \begin{cases} 1 - |u|, & \text{if } 0 \leqslant |u| \leqslant 1; \\ 0, & \text{otherwise.} \end{cases} \tag{3}$$

Additionally, piecewise cubic polynomials are frequently used to construct kernels. The piecewise cubic convolution (PCC) represented by piecewise cubic polynomials is

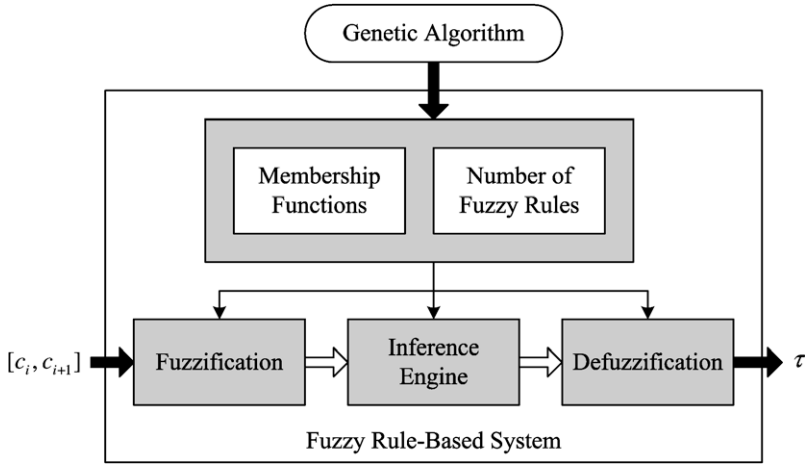


**Fig. 6.** The proposed fuzzy system combining with genetic learning algorithm.

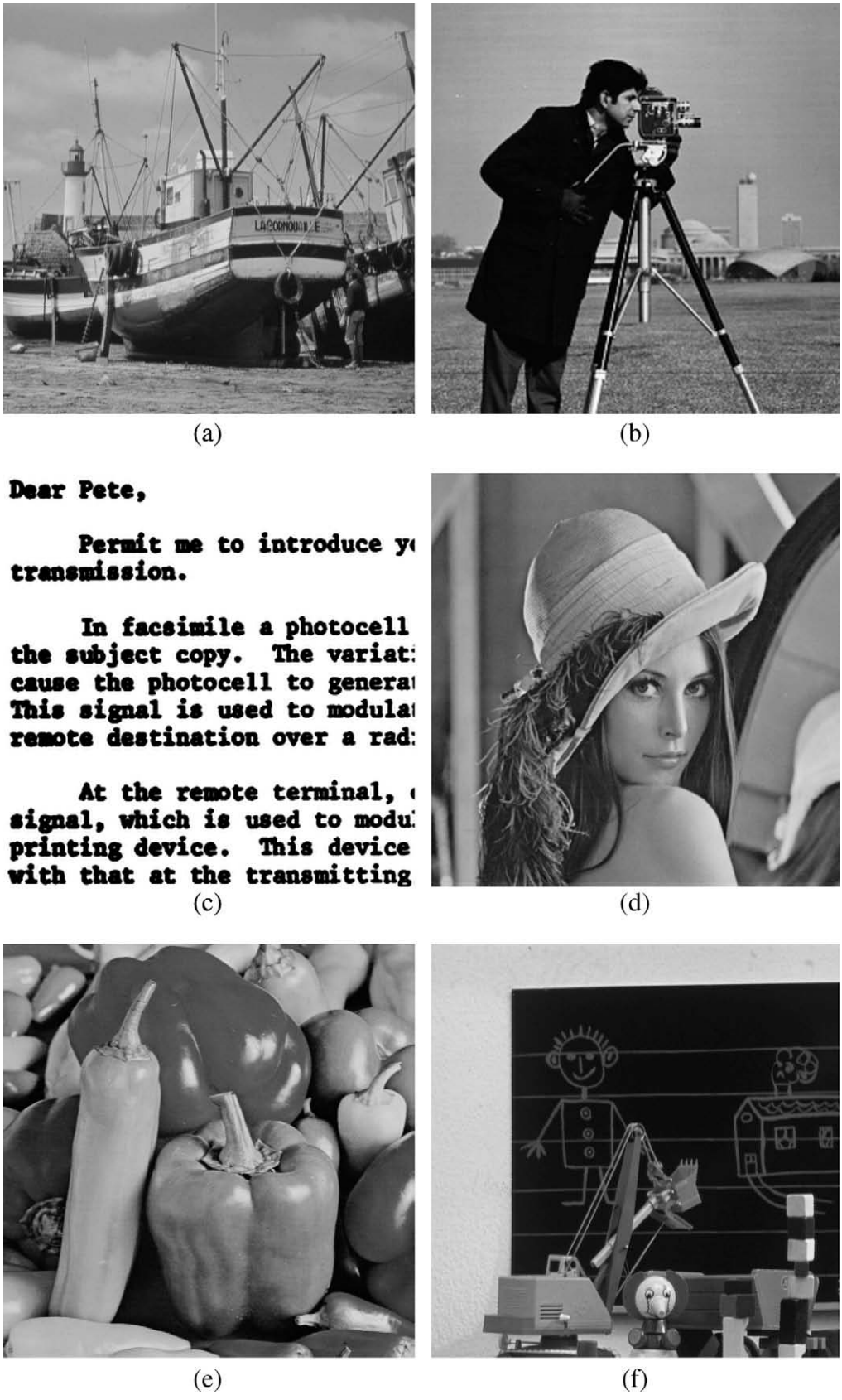


**Fig. 7.** Some test images: (a) boats, (b) cameraman, (c) fax, (d) Lena, (e) peppers, and (f) toys.

**Table 3**
Comparisons while LEAD impacting on different interpolation methods.

| Methods | Boats | Cameraman | Fax | Lena | Peppers | Toys | Average |
|---|---|---|---|---|---|---|---|
| *Without LEAD* | | | | | | | |
| Bilinear | 30.43 | 34.20 | 27.14 | 35.74 | 35.23 | 32.46 | 32.53 |
| Bicubic | 37.58 | 36.58 | 30.93 | 37.00 | 35.81 | 32.94 | 35.14 |
| Cubic Spline | 29.69 | 32.88 | 26.02 | 34.35 | 34.56 | 31.64 | 31.52 |
| *With LEAD* | | | | | | | |
| Bilinear | 30.73 | 36.43 | 30.03 | 36.76 | 36.21 | 33.17 | 33.89 |
| Bicubic | 37.69 | 37.78 | 32.88 | 37.35 | 36.33 | 33.49 | 35.92 |
| Cubic Spline | 29.94 | 34.16 | 27.17 | 35.11 | 35.37 | 32.15 | 32.32 |

$$\varphi_2(u)=\begin{cases}(a+2)|u|^3-(a+3)|u|^2+1, & \text{if } 0\leqslant|u|<1;\\ a|u|^3-5a|u|^2+8a|u|-4a, & \text{if } 1\leqslant|u|<2;\\ 0, & \text{otherwise.}\end{cases} \tag{4}$$

where constant $a$ denotes the slope of the PCC kernel at $u = 1$. When $a = -1/2$, this third-order kernel is called cubic convolution interpolation (also called bicubic in image interpolation). This field has been widely researched (Keys, 1981; Lehmann et al., 1999).

### 2.2. Motivation description

Consider the interested point $x \in [x_i, x_{i+1}]$ again, where a symmetric kernel $\varphi(u)$ is defined within a bounded interval $|u| \leqslant L$, and the kernel is zero outside this interval. Hence, Eq. (2) can be rewritten as

$$\begin{aligned}\tilde{f}_L(x) &= f(x_{i-L+1})\varphi(s+L-1)+\cdots+f(x_i)\varphi(s)+\cdots\\ &\quad +f(x_{i+L})\varphi(s-L)\\ &= \sum_{j=-L+1}^{L} f(x_{i+j})\varphi(s-j)\end{aligned} \tag{5}$$

where $L$ is a positive integer number denoting the half length of kernel. As indicated in Eq. (5), the interpolated value $\tilde{f}(x)$ is calculated as a weighted sum of the neighboring samples around point $x$.

As introduced in Subsection 2.1, the continuous result $\tilde{f}$ can be theoretically reconstructed by the sinc function as the interpolation kernel.

$$\begin{aligned}f(x) &= \tilde{f}_\infty(x) = \sum_{j=-\infty}^{\infty} f(x_{i+j})\varphi(s-j) = \sum_{j=-L+1}^{L} f(x_{i+j})\varphi(s-j)+\varepsilon_L\\ &= \tilde{f}_L(x)+\varepsilon_L\end{aligned} \tag{6}$$

and

$$\varepsilon_L = \sum_{j=-\infty}^{-L} f(x_{i+j})\varphi(s-j)+\sum_{j=L+1}^{\infty} f(x_{i+j})\varphi(s-j), \tag{7}$$

where the subscript $\infty$ means that the kernel length is infinite, and $\varepsilon_L$ denotes the error between $\tilde{f}_\infty(x)$ and $\tilde{f}_L(x)$. Since $f(x_{i+j})$ is available data at sampling node $x_{i+j}$, $\varepsilon_L = \varepsilon_L(s)$ is considered as a function of argument input $s$. Consider a new $s'$ to replace $s$ in Eq. (7), yielding

$$|\varepsilon_L| = \left|\sum_{j=-\infty}^{\infty} f(x_{i+j})\varphi(s'-j)-\sum_{j=-L+1}^{L} f(x_{i+j})\varphi(s'-j)\right| \tag{8}$$

be minimized ($\varepsilon_L$ is differentiable at $s'$). In Eq. (8), the value of $|\varepsilon_L|$ can be reduced by trying various real-valued $s'$. However, properly estimating of $s'$ to yield an accurate interpolated value is a significant issue. Fuzzy techniques have been extensively adopted over the past years in locating unknown systems (or functions) from known knowledge. The novelty underlying this study is to establish a fuzzy system for generating a new estimate of $s'$. This new estimated distance is then applied to numerous interpolation methods for producing high-qualified images.

## 3. Main algorithm

### 3.1. Configuration of the proposed fuzzy system

Most traditional interpolation methods are accurate enough for smooth regions in signals or images, but have difficulty in handling a 1D function containing a sharp transition, such as that shown in Fig. 1. In this function, the point $x_i$ locates at the edge, and the solid line represents an ideally reconstructed function for interpolation using involving samples $\{f(x_k)|k = i-1, i, i+1, i+2\}$. The edge is enhanced when the interpolated result approaches the ideal edge model. Using the simplest kernel defined in Eq. (3) for the explanation, $\tilde{f}_{L=1}(x) = (1-s)f(x_i)+sf(x_{i+1})$ follows from Eq. (5), where $x \in [x_i, x_{i+1}]$. Lowering the weight of $f(x_i)$ (on the sharp side), while raising the weight of $f(x_{i+1})$ (on the flat side) can yield a desired estimate of $\tilde{f}(x)$. The slope measure $c_\ell$ represents the local gradient at point $x_\ell$ ($\ell = i, i+1$), and is given by

$$c_\ell = |f(x_{\ell+1})-f(x_{\ell-1})|, \quad \text{for } \ell = i \quad \text{and } i+1. \tag{9}$$

Thus, the primary rule for tuning weights is that "If $c_\ell$ is small (or large), then the weight of $f(x_\ell)$ should be increased (or decreased)". Fig. 2a and b shows the relationship between $s$ and weights of $f(x_i)$ and $f(x_{i+1})$ of three representative methods, respectively. The depicted curves in Fig. 2 indicate that the weight of $f(x_i)$ monotonically decreases, and that of $f(x_{i+1})$ increases, as $s$ increases. Based on Fig. 2 and human intuition, the dual linguistic rules for tuning weights are established as the following IF-THEN form.

***Rule 1***: IF $c_i$ is small (or large), THEN $s$ should be decreased (or increased).
***Rule 2***: IF $c_{i+1}$ is small (or large), THEN $s$ should be increased (or decreased).

Consider a fuzzy system consisting of two inputs and a single output. Terms $c_i$ and $c_{i+1}$ denote the premise variables of each fuzzy rule, and $\tau$ denotes the consequent variable adopted to estimate $s'$. Let $s'$ be defined as

$$s' = f(s,\tau) = \begin{cases} s^\tau, & \text{if } c_i \leqslant c_{i+1};\\ 1-(1-s)^\tau, & \text{otherwise.}\end{cases} \tag{10}$$

Based on Eq. (10), the derived estimate $s'$, called locally edge-adapted distance (LEAD), is also in the range [0,1]. This study adopts the Mamdani-type model to describe the fuzzy rules. Therefore, the $r$th rule in the fuzzy rule base is described as

***Rule r***: IF $c_i$ is $\tilde{A}_{1r}$ AND $c_{i+1}$ is $\tilde{A}_{2r}$, THEN $\tau$ is $\tilde{B}_r$.

Where $\tilde{A}_{1r}$, $\tilde{A}_{2r}$, and $\tilde{B}_r$ belong to fuzzy sets $\{A_{11}, A_{12}, \ldots, A_{1M}\}$, $\{A_{21}, A_{22}, \ldots, A_{2M}\}$, and $\{B_1, B_2, \ldots, B_M\}$, respectively. Figs. 3 and 4 illustrate the fuzzy sets of premise and consequent variables partitioned in their corresponding universes of discourse. When a given input pair $[\tilde{c}_i, \tilde{c}_{i+1}]$ goes into the constructed fuzzy rules, the final output $\tilde{\tau}$ is derived via minimum inference engine and center-of-gravity defuzzification method:

$$\tilde{\tau} = \frac{\int \tau \cdot \hat{B}(\tau)d\tau}{\int \hat{B}(\tau)d\tau} \tag{11}$$

and

$$\hat{B}(\tau) = \max_{n=1}^{M^2}\left\{\tilde{A}_{1n}(\tilde{g}_i)\wedge\tilde{A}_{2n}(\tilde{g}_{i+1})\wedge\tilde{B}_n(\tau)\right\}, \tag{12}$$

where $M^2$ denotes the total number of non-conflicting fuzzy rules, since each premise variable is partitioned into $M$ fuzzy sets, and $\wedge$ denotes the minimum operator. The derived final output $\tilde{\tau}$ is then substituted for $\tau$ in Eq. (10) to determine the calculate the result of $s'$.

### 3.2. Genetic learning algorithm

Genetic algorithm (GA) is a search and optimization technique based on natural selection and genetic rules (Srinivas & Patnaik, 1994). A simple GA procedure starts with a population

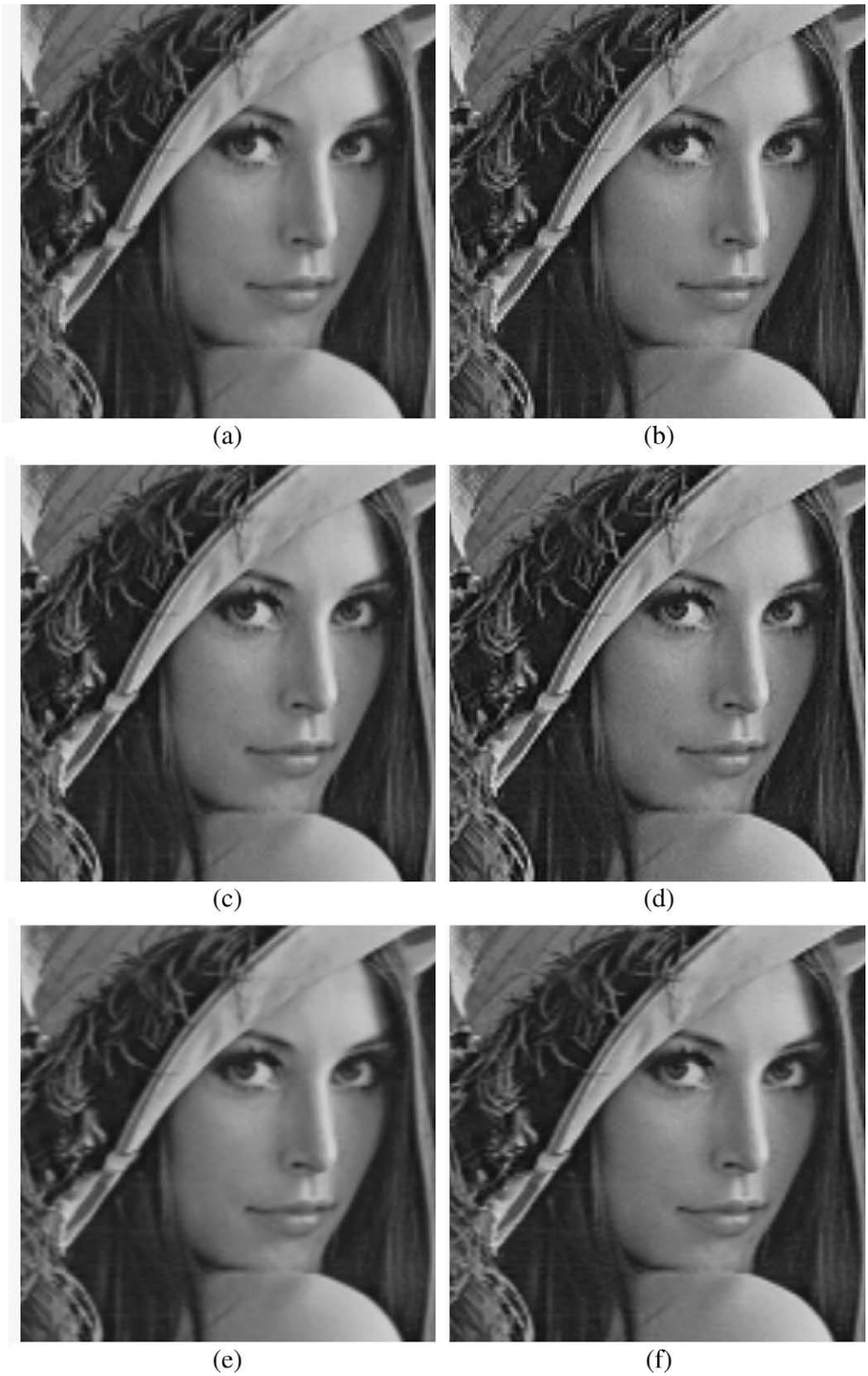


**Fig. 8.** Portions of reconstructed *Lena* image: (a) Bilinear, (b) LEAD–Bilinear, (c) Bicubic, (d) LEAD–Bicubic, (e) Cubic Spline, and (f) LEAD–Cubic Spline.

of solutions (called chromosomes) that constitutes the first generation and undergoes evolution. In this subsection, GA is adopted to generate the critical parameters of the proposed fuzzy system automatically. The critical parameters are: (1) the universe of discourse of consequent variable, (2) the number of labels for each variable, and (3) the critical points of fuzzy sets. The GA in this subsection is called a "genetic learning algorithm" (GLA).

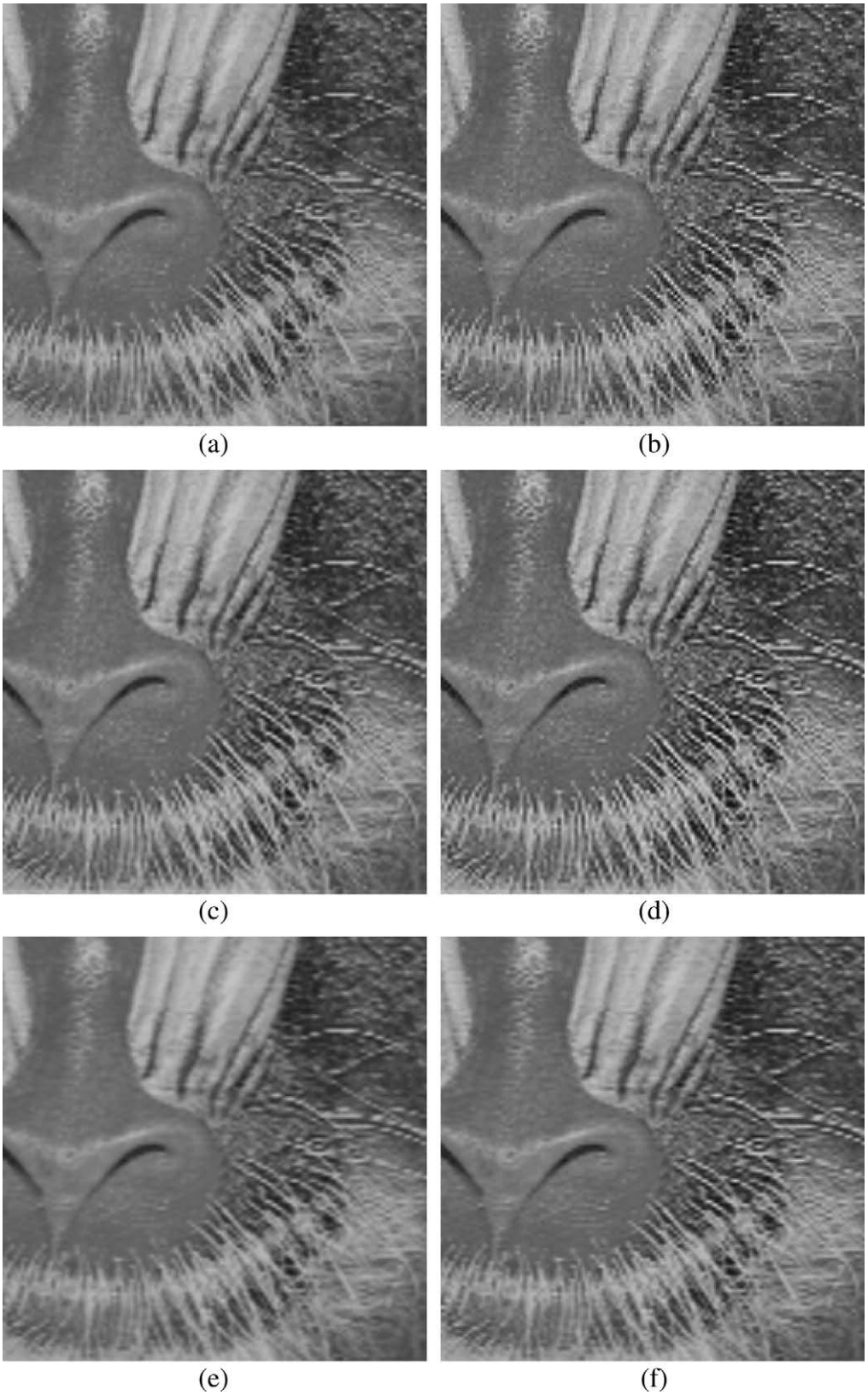


**Fig. 9.** Portions of reconstructed *Baboon* image: (a) Bilinear, (b) LEAD–Bilinear, (c) Bicubic, (d) LEAD–Bicubic, (e) Cubic Spline, and (f) LEAD–Cubic Spline.

Table 1 shows the fuzzy rule table, which is predefined according to given knowledge in order to reduce the computation effort of GLA. Figs. 3 and 4 show the fuzzy sets $\{A_{11},A_{12},\dots A_{1M}\}$, $\{A_{21},A_{22},\dots A_{2M}\}$ and $\{B_1,B_2,\dots B_M\}$. To fully characterize the proposed fuzzy system except the predefined rule base, the number of labels of each linguistic term $M$, the base lengths of membership functions $\{\alpha_1,\alpha_2,\dots \alpha_M\}$ and $\{\beta_1,\beta_2,\dots \beta_{M-1}\}$ with constraints $\alpha_1+\alpha_2+\cdots+\alpha_M=c_{\max}$ and $\beta_1+\beta_2+\cdots+\beta_{M-1}=\tau_{\max}$ must be obtained in advance. Here, $c_{\max}$ denotes the maximum of premise variables, and $c_{\max}=2^8-1$ to represent the 8-bit gray images used in the simulation. The universe of discourse of the consequent variable is set as $[0,\tau_{\max}]$. To reduce the learning complexity, $M$ is restricted to being an integer in the interval [2,5]. Accordingly, the procedure of GLA to optimize the parameters for the proposed fuzzy system for all possible values of $M$ is presented below (see Fig. 5).

1. Create an initial population $P(0)$ of $K$ solutions randomly ($K=20$ in this study). Each member of solutions is encoded as the chromosome illustrated in Fig. 5.
2. Evaluate each solution, and calculate its corresponding fitness value $\tilde{J}$.
3. Utilize $\tilde{J}$ to select a subset of solutions via well-known "Roulette wheel selection".
4. Produce a new generation $P(t)$ of $K$ solutions by applying genetic operators, including reproduction, crossover and mutation.
5. Repeat steps 2–4 until either the optimal fitness value is obtained, or an upper limit on the number of generations is achieved.

This paragraph presents a mathematical model as the ideal function to evaluate the effectiveness of the fuzzy system while the parameters are optimizing via GLA. First, a sigmoid function having a sharp transition region is created to be the ideal function and is given by

$$f(x)=\frac{b}{1+e^{-\lambda x}}, \tag{13}$$

where $x\in[-\Gamma,\Gamma]$. The constant $\lambda$ controls the sharpness of transition region, and $b$ denotes the transition magnitude. This study adopted $\lambda=5$, $b=255$ and $\Gamma=5$ to simulate an extremely sharp region in an 8-bit gray image. A good interpolation should have a small mean squared error between the interpolated result and the ideal function. The mean squared error is defined as $MSE=\frac{1}{2\Gamma}\int_{-\Gamma}^{\Gamma}\left[f(x)-\tilde{f}_L(x)\right]^2dx$, where $\tilde{f}_L(x)$ denotes the estimated value by interpolation. Hence, the inverse of the mean squared error is adopted as the fitness function $\tilde{J}=MSE^{-1}$. Notably, the critical parameters are individually optimized for different interpolation methods. Table 2 presents the optimized parameters for the three representative interpolation methods used in experimental simulations of this work. Fig. 6 shows the essential conception of the proposed fuzzy system combining with GLA.

### 3.3. Computation reduction

Fuzzification, rule activation, fuzzy inference and defuzzification are performed to derive the final output when the inputs go into a fuzzy system. To reduce computational burden, the proposed fuzzy system is considered as a mapping function representing the input–output relationship $\tau=g(c_i,c_{i+1})$. For a specified interpolation in gray images, this relationship function can be pre-obtained and represented as a $256\times256$ look-up table, since the inputs are simply integers in the range [0,255]. Therefore, deriving the final output $\tilde{\tau}$ for a given input vector is very easy and fast.

## 4. Experimental results

The generated locally edge-adapted distance (LEAD) derived via genetic fuzzy system was adopted to replace the original normalized Euclidean distance in the bilinear, bicubic, and cubic spline interpolation formulae. Those selected interpolation methods are well-known, and practicable to enlarge an image by any magnification factor along each dimension. The comparisons were performed by evaluating the results of each method without and with LEAD. Fig. 7 shows some test images ($512\times512$ pixels). Each test image was first down-sampled by a factor $1/\kappa$, and then enlarged by a factor $\kappa$ using a specified interpolation method. Thus, the peak signal-to-noise ratio (PSNR) value between the original image and the enlarged image was calculated to evaluate the performance of each interpolation method. Table 3 lists the PSNR comparisons with $\kappa=2$. The upper part of the table shows the results by traditional interpolations. The bottom part shows the interpolation results of the proposed LEAD, which are obviously better than those of the traditional methods. The average improved PSNRs were in the range 0.8–1.3 dB. Fig. 8 shows a portion of the reconstructed HR *Lena* image: Fig. 8a–f, respectively, show the results of reconstruction by bilinear, bilinear with LEAD (LEAD–Bilinear), bicubic, bicubic with LEAD (LEAD–Bicubic), cubic spline, and cubic spline with LEAD (LEAD–Cubic Spline) interpolation methods. Similarly, Fig. 9 shows a portion of the reconstructed HR *Baboon* image containing many sharp edges, with a non-integer factor $\kappa=1.8$. This figure particularly demonstrated the superior effectiveness of LEAD in preserving locally detailed information over the traditional interpolation approaches.

Additionally, LEAD–Bilinear method was compared with three other recently developed bilinear-based interpolation methods, namely WaDi-Bilinear interpolation (Ramponi, 1999), Adaptive–Bilinear interpolation (Huang & Lee, 2004) and CFLS–Bilinear (Yoo, 2007) interpolation methods. The similar testing procedure, containing down-sampling and expanding operations, was applied to measure the effectiveness of each interpolation method. Table 4

**Table 4**
Comparison of different bilinear-based interpolation method.

| Methods | Boats | Cameraman | Fax | Lena | Peppers | Toys | Average |
|---|---|---|---|---|---|---|---|
| *The magnification factor* $\kappa=1.5$ | | | | | | | |
| WaDi–Bilinear | 32.46 | 36.44 | 28.52 | 37.08 | 36.69 | 34.27 | 34.24 (2) |
| Adapt–Bilinear | 31.77 | 35.33 | 25.81 | 36.32 | 36.35 | 34.07 | 33.28 (4) |
| CFLS–Bilinear | 31.95 | 35.14 | 26.94 | 36.24 | 35.65 | 34.01 | 33.32 (3) |
| LEAD–Bilinear | 32.74 | 36.97 | 28.82 | 37.56 | 37.02 | 34.72 | 34.64 (1) |
| *The magnification factor* $\kappa=2$ | | | | | | | |
| WaDi–Bilinear | 30.58 | 35.44 | 30.09 | 36.27 | 35.68 | 33.00 | 33.51 (3) |
| Adapt–Bilinear | 30.46 | 34.38 | 27.21 | 35.93 | 36.15 | 33.23 | 32.89 (4) |
| CFLS–Bilinear | 29.94 | 36.08 | 30.64 | 36.23 | 35.37 | 33.15 | 33.57 (2) |
| LEAD–Bilinear | 30.73 | 36.43 | 30.03 | 36.76 | 36.21 | 33.17 | 33.89 (1) |

shows the PSNR comparisons with factors $\kappa = 1.5$ (non-integer factor) and $\kappa = 2$ (integer factor). The last column in this table presents the average PSNR for each method, and their performance ranking. This table indicates that the proposed LEAD is consistently better than other approaches in different magnification factors. Fig. 10 shows a portion of the reconstructed HR *Boats* image by

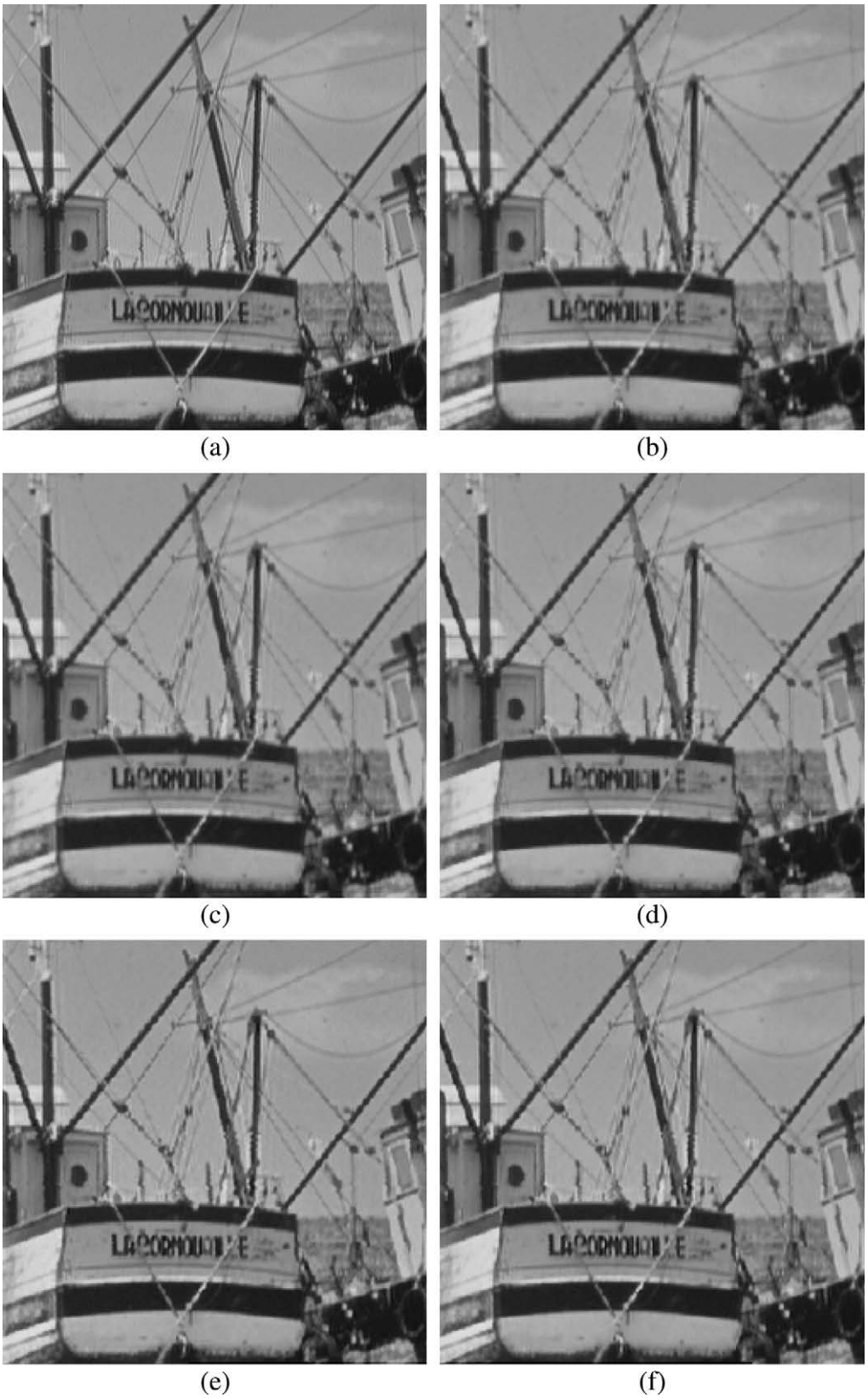


**Fig. 10.** Portions of reconstructed *Boats* image: (a) Original, (b) Bilinear, (c) WaDi–Bilinear, (d) Adapt–Bilinear, (e) CFLS–Bilinear, and (f) LEAD–Bilinear.

different interpolation algorithms: Fig. 10a shows the original image, and Fig. 10b–f shows the reconstructed image obtained by Bilinear, WaDi–Bilinear, Adapt–Bilinear, CFLS–Bilinear, and the proposed LEAD–Bilinear methods, respectively.

## 5. Conclusions

This study has presented a new adaptive framework for estimating a locally edge-adapted distance by combining fuzzy logics with genetic learning algorithm. The new derived distance improves the efficiency of traditional methods for sharp regions via considering the local gradients around a point of interest. Moreover, the critical parameters of the constructed fuzzy system for various interpolation methods could be optimized by the presented genetic learning procedure. The comparative PSNR values demonstrate that the proposed locally edge-adapted distance is effective when employing a specified interpolation to reconstruct HR images. Therefore, this study presents a reliable method for enhancing traditional image interpolation methods.

## Acknowledgement

The authors would like to thank the National Science Council of the Republic of China, Taiwan, for financially supporting this research under the Grant NSC-96-2221-E-027-136.

## References

Aràndiga, F., Donat, R., & Mulet, P. (2003). Adaptive interpolation of images. *Signal Processing, 83*(2), 459–464.

Battiato, S., Gallo, G., & Stanco, F. (2002). A locally adaptive zooming algorithm for digital images. *Image and Vision Computing, 20*(11), 805–812.

Carey, W. K., Chuang, D. B., & Hemami, S. S. (1999). Regularity-preserving image interpolation. *IEEE Transactions on Image Processing, 8*(9), 1293–1297.

Carrato, S., Ramponi, G., & Marsi, S. (1996). A simple edge-sensitive image interpolation filter. In *Proceedings of international conference on image processing, Lausanne* (pp. 711–714).

Carrato, S., & Tenze, L. (2000). A high quality 2× image interpolator. *IEEE Signal Processing Letters, 7*(6), 132–134.

Cha, Y. J., & Kim, S. J. (2007). The error-amended sharp edge (EASE) scheme for image zooming. *IEEE Transactions on Image Processing, 16*(6), 1496–1505.

Chang, S. G., Cvetković, Z., & Vetterli, M. (2006). Locally adaptive wavelet-based image interpolation. *IEEE Transactions on Image Processing, 15*(6), 1471–1485.

Chen, M. J., Huang, C. H., & Lee, W. L. (2005). A fast edge-oriented algorithm for image interpolation. *Image and Vision Computing, 23*(9), 791–798.

El-Khamy, S. E., Hadhoud, M. M., Dessouky, M. I., Salam, B. M., & Abd El-Samie, F. E. (2005). Efficient implementation of image interpolation as an inverse problem. *Digital Signal Processing, 15*(2), 137–152.

Hong, S. H., Park, R. H., Yang, S. J., & Kim, J. Y. (2008). Image interpolation using interpolative classified vector quantization. *Image and Vision Computing, 26*(2), 228–239.

Huang, J. W., & Lee, H. S. (2004). Adaptive image interpolation based on local gradient features. *IEEE Signal Processing Letters, 11*(3), 359–362.

Keys, R. G. (1981). Cubic convolution interpolation for digital image processing. *IEEE Transactions on Acoustics, Speech, and Signal Processing, 29*(6), 1153–1160.

Lehmann, T. M., Gönner, C., & Spitzer, K. (1999). Survey: Interpolation methods in medical image processing. *IEEE Transactions on Medical Imaging, 18*(11), 1049–1075.

Li, X., & Orchard, M. T. (2001). New edge-directed interpolation. *IEEE Transactions on Image Processing, 10*(10), 1521–1527.

Meijering, E., & Unser, M. (2003). A note on cubic convolution interpolation. *IEEE Transactions on Image Processing, 12*(4), 477–479.

Muresan, D. D., & Parks, T. W. (2004). Adaptively quadratic (AQua) image interpolation. *IEEE Transactions on Image Processing, 13*(5), 690–698.

Plaziac, N. (1999). Image interpolation using neural networks. *IEEE Transactions on Image Processing, 8*(11), 1647–1651.

Ramponi, G. (1999). Warped distance for space-variant linear image interpolation. *IEEE Transactions on Image Processing, 8*(5), 629–639.

Reichenbach, S. E., & Geng, F. (2003). Two-dimensional cubic convolution. *IEEE Transactions on Image Processing, 12*(8), 857–865.

Sheppard, D. G., Panchapakesan, K., Bilgin, A., Hunt, B. R., & Marcellin, M. W. (2000). Lapped nonlinear interpolative vector quantization and image super-resolution. *IEEE Transactions on Image Processing, 9*(2), 295–298.

Shi, J. Z., & Reichenbach, S. E. (2006). Image interpolation by two-dimensional parametric cubic convolution. *IEEE Transactions on Image Processing, 15*(7), 1857–1870.

Sigitani, T., Iiguni, Y., & Maeda, H. (1999). Image interpolation for progressive transmission by using radial basis function networks. *IEEE Transactions on Neural Networks, 10*(2), 381–390.

Srinivas, M., & Patnaik, L. M. (1994). Genetic algorithms: A survey. *Computer, 27*(6), 17–26.

Tafti, P. D., Shirani, S., & Wu, X. L. (2006). On interpolation and resampling of discrete data. *IEEE Signal Processing Letters, 13*(12), 733–736.

Temizel, A., & Vlachos, T. (2006). Wavelet domain image resolution enhancement. *IEE Proceedings of Vision Image Signal Processing, 153*(1), 25–30.

Wang, Q., & Ward, R. K. (2007). A new orientation–adaptive interpolation method. *IEEE Transactions on Image Processing, 16*(4), 889–900.

Yoo, H. (2007). Closed-form least-squares technique for adaptive linear image interpolation. *Electronics Letters, 43*, 210–212.

Zhang, L., & Wu, X. (2006). An edge-guided image interpolation algorithm via directional filtering and data fusion. *IEEE Transactions on Image Processing, 15*(8), 2226–2238.